Temperature dissipation fluctuations in a turbulent boundary layer

K. R. Sreenivasan and R. A. Antonia

Department of Mechanical Engineering, University of Newcastle, New South Wales, 2308, Australia

H. Q. Danh

Department of Mechanical Engineering, University of Sydney, New South Wales, 2006, Australia
(Received 27 September 1976; final manuscript received 15 March 1977)

All three components of the dissipation rate of the fluctuating temperature θ are measured simultaneously in the inner region of a fully developed turbulent boundary layer at a moderate Reynolds number. Measurements are made with a probe of four cold wires consisting of two closely spaced parallel vertical wires mounted a small distance upstream of two closely spaced parallel horizontal wires. In the inner region of the layer, local isotropy is not closely approximated $[\overline{(\partial\theta/\partial z)^2} > \overline{(\partial\theta/\partial y)^2} > \overline{(\partial\theta/\partial x)^2}]$. The spectral density of the sum $\chi[=(\partial\theta/\partial x)^2+(\partial\theta/\partial y)^2+(\partial\theta/\partial z)^2]$ is similar in shape to that of $(\partial\theta/\partial y)^2$ or $(\partial\theta/\partial z)^2$, but not as rich in high frequency content as that of $(\partial\theta/\partial x)^2$. The probability density of χ has a lower skewness and flatness factor and is more closely log-normal than those of the individual components. This is true regardless of whether χ and its components are unaveraged or locally averaged over a linear dimension r. When averaging is applied, departures from log-normality are diminished but do not disappear entirely. The variance σ^2 of the logarithm of the locally averaged χ is proportional to $\ln r$ over a wide range of r ($r_{max}/r_{min} \simeq 30$), in contrast to the individual components where this ratio may be as small as 2. The value of the Kolmogoroff constant μ_θ determined from the slope of σ^2 vs $\ln r$ is about 0.35. This is consistent with the slope of the spectral density of χ and is also in agreement with previous best estimates of μ_θ (and μ) obtained at high Reynolds numbers.

I. INTRODUCTION

There has been a great deal of interest in the statistics of the fine scale structure of turbulence, particularly in view of the observed spatial intermittency of ϵ, the rate of dissipation of turbulent energy fluctuations. Several models have been suggested which incorporate this intermittency explicitly. Kolmogoroff[1] and Obukhov[2] hypothesized that ϵ_r, the average of ϵ over a volume of linear dimension r ($\eta \ll r \ll L$, where η is the Kolmogoroff length and L is an integral length scale of turbulence) is log-normally distributed and that the variance of $\ln\epsilon_r$ decreases linearly with $\ln r$. Together these are often referred to as Kolmogoroff's third hypothesis.

Several attempts have been made to verify this hypothesis. They invariably assume that $(\partial u/\partial x)^2$, the squared streamwise velocity derivative, is representative of ϵ. Since $\epsilon=(\nu/2)(\partial u_i/\partial x_j+\partial u_j/\partial x_i)^2$, it is unreasonable to expect the statistics of instantaneous values of $(\partial u/\partial x)^2$ to be representative of those of ϵ. A very important reason for this, as pointed out by Gibson and Masiello,[3] is that contributions to ϵ come largely from cross terms when $(\partial u/\partial x)^2$ is small, which makes $(\partial u/\partial x)^2$ nonrepresentative of ϵ. It, therefore, follows that a valid check of Kolmogoroff's third hypothesis cannot be strictly made with information relating to $(\partial u/\partial x)^2$, particularly when $(\partial u/\partial x)^2$ is small.

A basis for Kolmogoroff's hypothesis has been provided by the arguments put forward by Yaglom[4] and Gurvich and Yaglom.[5] Their arguments are equally applicable to a locally averaged dissipation of scalar fluctuations (see, e.g., Masiello[6]). In the case of temperature fluctuations θ, the dissipation $\chi=2\alpha(\partial\theta/\partial x_i)^2$, where α is the thermal diffusivity, contains only three components instead of the nine in ϵ. Gibson and Masiello[3] argue that the components of χ are of the same order of magnitude for all χ, and that the absence of cross terms in χ makes a component of χ such as $(\partial\theta/\partial x)^2$ more representative of χ than $(\partial u/\partial x)^2$ is of ϵ. While this is true, the other objection raised by Gibson and Masiello persists: The sum of several log-normal random variables need not be log-normal and vice versa, unless the random variables are all identical (not merely in the statistical sense). Therefore, a very good case exists for testing Kolmogoroff's hypothesis on χ by measuring all three of its components simultaneously.

In this paper, we present measurements of all three components of χ in a fully developed thermal boundary layer. Section II contains details of the experimental arrangement and technique, and an assessment of the measuring techniques is given in Sec. III. In Secs. IV and V, the statistics of χ and its components are examined in relation to Kolmogoroff's third hypothesis.

II. EXPERIMENTAL ARRANGEMENT

The wind tunnel and the heating arrangement used for the present investigations are described in Antonia *et al.*[7] Briefly, the tunnel has a 38 cm wide, 23 cm working section which is 4.9-m long. The first 2 m of the asbestos floor of the working section are unheated. The remainder of the floor is the heated section made up of identical spanwise strips of Inconel cemented to a Sindanyo base, connected in series. The floor is heated by an ac source of 60 A at 6 V. About 30 min of tunnel running time are required to establish stable and uniform heating conditions of constant surface heat flux.

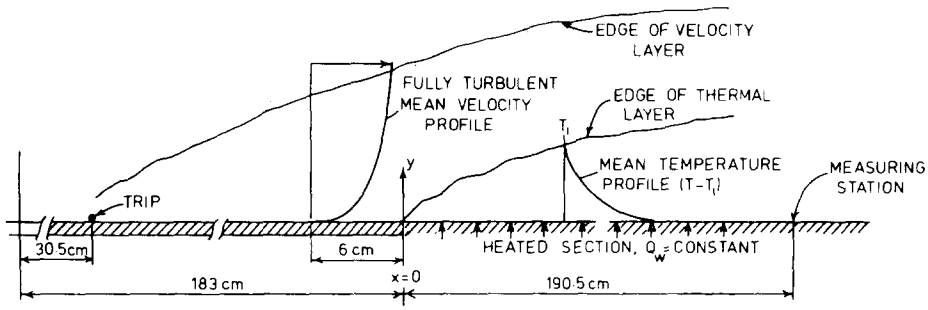

FIG. 1. Schematic diagram of experimental arrangement.

Measurements are made at a station $x = 190.5$ cm (see Fig. 1), where the thermal layer is fully submerged in the velocity boundary layer. At the measuring station, the thermal thickness δ_t (where 99.5% of the total temperature difference is attained) is 66 mm and the velocity boundary layer thickness δ (where 99.5% of the free-stream velocity is attained) is 86 mm, when the tunnel is operated at a nominal free-stream velocity U_∞ of 9.45 m sec^{-1}. Under these operating conditions, the wall temperature T_w is about 12 °C above ambient and the Reynolds number based on the momentum thickness is 5730. Earlier measurements reported by Antonia *et al.*[7] have established that the thermal boundary layer is approximately self-preserving at $x = 190.5$ cm.

All three components of temperature "dissipation" fluctuations are obtained simultaneously with a four-wire probe which consists of two horizontal wires parallel to the wall, separated by a vertical distance of 1.2 mm, and two other parallel vertical wires normal to the wall, separated by a horizontal spanwise distance of 0.9 mm. The horizontal wires are mounted on a modified miniature DISA X probe while the vertical wire pair consists of two single wires, mounted on separate right angle probes, and is located 0.6 mm in front of the plane of the horizontal wires (see Fig. 2).

All temperature wires are made of 0.6 μm diam platinum wires of about 0.8 mm in length; they are operated "cold" at a constant current of 0.1 mA with the use of four channels of a six-channel constant current anemometer.[7] The low value of operating current insures that the wires are sensitive only to temperature fluctuations. The resistances of the two wires in either pair (nominally about 650Ω) are matched to within 3%.

The outputs of the two horizontal wires and the two vertical wires are subtracted with the use of two DISA 55D26 signal conditioners, whose outputs are assumed to be directly proportional to $\partial\theta/\partial y$ and $\partial\theta/\partial z$, respectively. The signal $\partial\theta/\partial x$ is obtained by differentiating, with respect to time, the output of the upper horizontal wire and using Taylor's hypothesis. (The coordinates x and y are shown in Fig. 1, and z is in the spanwise direction.) The extent of validity of these approximations is discussed in Sec. III. Root-mean-square values of the temperature signals, the differences, and the time derivative are read on a DISA 55D35 rms meter. Temperature signals from all four wires, the two temperature differences and the derivative $\partial\theta/\partial x$ are recorded on a Philips ANALOG 7 FM tape recorder at a speed of 76.2 cm sec^{-1}. The tape recorder response is flat up to 10 kHz while the maximum Kolmogoroff frequency of the flow is 7.6 kHz. The tape recorder has a dynamic range of ± 5 V and a nominal signal/noise ratio of 40 dB.

Recorded signals are played back at a tape speed of 2.38 cm sec^{-1}, and signals proportional to $\partial\theta/\partial x$, $\partial\theta/\partial y$, and $\partial\theta/\partial z$ digitized at a frequency of 630 Hz. This corresponds to a real time frequency of 20160 Hz, which is somewhat higher than twice the maximum value of the Kolmogoroff frequency at the measurement station. Digital records used to compute statistics of dissipation are 332 800 characters long, equivalent to a real time duration of 16.5 sec. Averaging of χ or its components is performed over a time interval varying between 1 and 300 digital samples (each digital sample = 20 160^{-1} sec).

The temperature coefficient of resistance of the wires is found to be 0.0014 °C^{-1} by direct calibration in the potential core of an axisymmetric jet heated to about 30 °C above ambient temperature. The mean temperature profile in the thermal layer is obtained by taking only the dc output of one of the horizontal wires, which is read out on a digital voltmeter.

III. ERROR ESTIMATES

A. Interference effects

As mentioned in Sec. II, the three spatial derivatives of temperature are approximated by

$$\theta_x \equiv \partial\theta/\partial x \simeq -U^{-1}(\partial\theta/\partial t)\,, \tag{1}$$

$$\theta_y \equiv \partial\theta/\partial y \simeq (\Delta\theta)_h/\Delta y\,, \tag{2}$$

and

$$\theta_z \equiv \partial\theta/\partial z \simeq (\Delta\theta)_v/\Delta z\,, \tag{3}$$

where U is the local mean velocity and the suffixes h

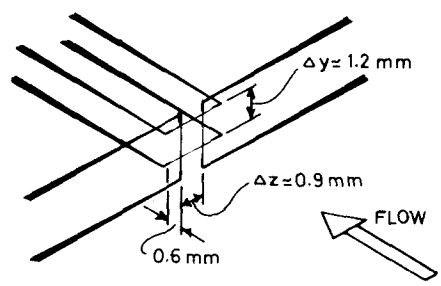

FIG. 2. Schematic of the four-wire probe.

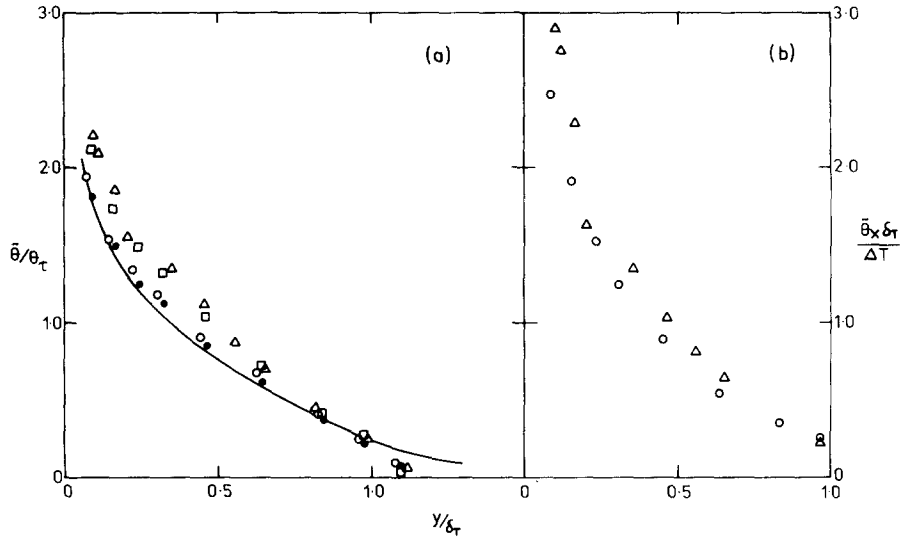

FIG. 3. (a) Comparison of temperature root-mean-square values obtained with four-wire and two-wire probes. Four wire probe: ○, Bottom wire: ●, top wire: □, average of the vertical wires: △, two-wire probe data. ——Antonia *et al.*[7] (b) Comparison of rms values of streamwise derivative of temperature obtained with four-wire and two-wire probes. ○, four-wire probe; △, two-wire probe. ΔT is the difference between wall and ambient temperatures.

and v refer to the horizontal and vertical wire pairs, respectively. Equation (1) is assumed to be valid for relatively small turbulence levels. For the other two derivatives, the separation distances Δy and Δz must be small enough to justify approximations (2) and (3), but large enough to avoid excessive interference effects. (Incidentally, we note that, although the vertical and horizontal wire pairs bear a geometrical resemblance to the X-wire configuration, the cross talk between the two wires of an X probe of the type studied by Wyngaard,[8] or the changes in sensitivity coefficient noted by Strohl and Comte-Bellot,[9] are irrelevant to the present study where no quantity is obtained by "synthesis" of two signals, as in the case of an X wire.) An "optimum" choice is made here and the "residual" interference effects are estimated.

First, consider the vertical wires which yield θ_v. The two possible ways in which they can be affected are by mutual interference and by the aerodynamic effects of the probe and prongs carrying the horizontal wires (e.g., due to displacement of streamlines). For the probe configuration used here, the streamwise distance between the plane of the vertical wires and that of the horizontal wires is about $3\eta_\theta$ (where η_θ is the so-called Corrsin–Obukhov scale, $=1.28\eta$, where η is the Kolmogoroff length scale) and is, therefore, small compared with a scale characteristic of the flow development. It is of interest to note that Champagne *et al.*[10] studied the correlation between the intensities of two hot wires, one of which was placed directly in the wake of the other, and found that the optimum separation distance was about 3.5η. The horizontal wires are soldered at the tip of 8 mm long needles (< 0.5 mm diam at base) while the diameter of the supporting stem is 2 mm. It is thus unlikely that the aerodynamic effects will be serious. In fact, Strohl and Comte-Bellot[9] have investigated these effects on similar hot-wire X probes and concluded that these effects will be less than 5% on the hot-wire signals.

In relation to the influence of one wire on a neighboring wire, Tritton[11] has observed that the intensity of a hot wire reading is seriously reduced by the presence of another probe situated in its vicinity. For example, close to the wall ($y^+ = yU_\tau/\nu \simeq 20$), he noted as much as a 30% reduction in the root-mean-square intensity of streamwise velocity fluctuations sensed by a hot-wire when an X-wire probe was placed in its vicinity. This effect is considerably smaller with increasing distance from the wall. Our nearest measurement to the wall is at $y^+ \simeq 120$, where Tritton's own estimates (which must be considered to provide a conservative estimate for the likely error, considering that the present probe has a much slimmer stem and is farther away from the sensing element than in Tritton's case) suggest an error in the root-mean-square intensity of the order of 5%.

However, the same assertion cannot be made of the downstream influence of the vertical wires and their supports on the horizontal wires. The signals from the horizontal wires have therefore been examined without the vertical wires, by varying the distance Δy between them. (These data are referred to subsequently as the two-wire data.) The purpose of the latter investigation is to examine the effect on the signals of variable separation distance and to obtain data from interference-free probe. One wire is fixed close to the wall, while the other is traversed directly above it by means of an independent micrometer arrangement. Therefore, except for the measurements closest to the wall (which are discussed in the next section), the fixed wire is sufficiently distant from the moving wire (approximate separation distance being the height above the wall of the moving wire) for the measurements of the latter wire to be considered as free from interference.

Figure 3(a) gives a profile of $\tilde{\theta}$, the root-mean-square value of θ (normalized by the friction temperature $\theta_\tau = Q_w/U_\tau$, where Q_w is the wall heat flux) obtained from the two- and four-wire probes, with the same separation distance, Δy. (Here, $Q_w = 0.23$ m sec^{-1} °C and $U_\tau = 0.35$ m sec^{-1}.) For $y/\delta_t \lesssim 0.75$, it is clear that the values obtained by the two horizontal wires of the four-wire probe, while agreeing between themselves, are 10%–15% less than the corresponding two-wire probe values. It is interesting to note, however, that they

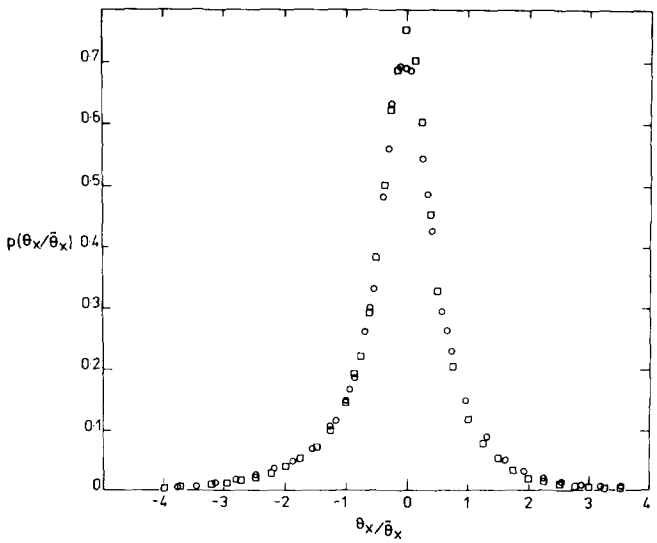

FIG. 4. Normalized probability density of θ_x obtained with two-wire and four-wire probes. o, four-wire probe data; □, two-wire probe data.

agree with the data of Antonia *et al.*[7] who used a two-wire probe similar to the present, with a fixed separation distance of the same order as in the present four-wire probe. It is also worth noting that the average of the vertical wire readings is in reasonable agreement with the two-wire data thus partially confirming our earlier conclusion that the vertical wire data are not seriously affected. There are, however, no significant differences among the various data for $y \gtrsim 0.75\delta_t$. A check on the derivatives [Fig. 3(b)] obtained from the two-wire and four-wire data shows a reduction of the same order in the root-mean-square values obtained by the horizontal wires of the four-wire probe.

To examine whether the previous effects are brought

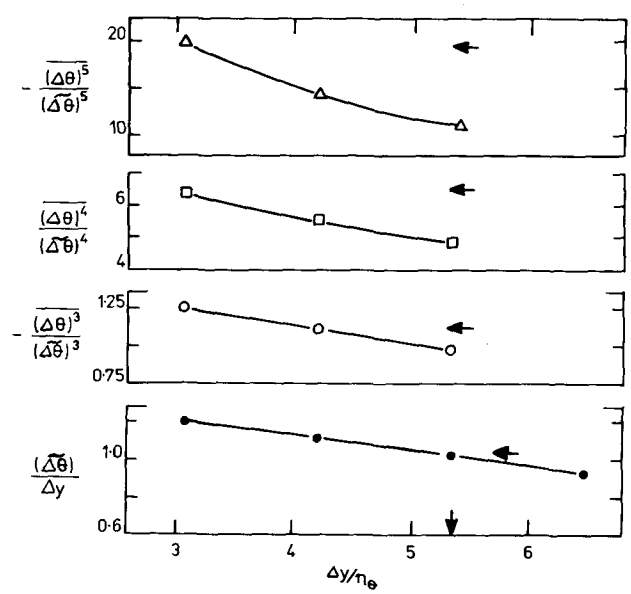

FIG. 5. Effect of variation of vertical separation distance on the moments of θ_y. ↓ and ← indicate the separation distance and the corresponding value of the moment, respectively, for the four-wire probe.

TABLE I. Basic flow parameter data at the measurement station. l_w is the length of the wire.

y/δ	U/U_∞	$(T_w-T)/T_w$	$\tilde{\theta}/T_w$	$\tilde{\theta}_x$	$\tilde{\theta}_y$	$\tilde{\theta}_z$	R_λ	η_θ/l_w
				(°C mm^{-1})				
0.06	0.61	0.78	0.110	0.54	0.61	0.70	135	0.20
0.12	0.68	0.85	0.085	0.43	0.46	0.49	153	0.22
0.18	0.71	0.89	0.074	0.34	0.37	0.40	169	0.25
0.24	0.75	0.91	0.065	0.28	0.30	0.34	175	0.27

about by a simple attenuation of the signal amplitude or by more detailed changes in the statistical properties of the signal, the probability density of θ_x obtained, using Eq. (1), from the upper wire of the two-wire probe is compared in Fig. 4 with that similarly obtained from the upper horizontal wire of the four-wire probe. The close agreement between them, except perhaps at the peak, suggests that the presence of the pair of vertical wires produces interference effects of a rather simple nature on the horizontal wires of the four-wire probe located downstream.

B. Effect of finite separation

Figure 5 shows the effect of the separation distance Δy on the higher order moments of θ_y obtained by Eq. (2); the data are from the first few measurements close to the wall made with the two-wire probe. The corresponding separation distance ($= 5.25\eta_\theta$) and the moments for the four-wire data are also shown. Simple extrapolation to $\Delta y = 0$ suggests that with the four-wire probe $\tilde{\theta}_y$ is likely to have been underestimated by about 20%; the normalized third, fourth, and fifth order moments seem to be, respectively, about 80%, 50%, and 30% of the limiting values ($\Delta y = 0$). Similar estimates are also likely to hold for θ_z. Note that the magnitude by which $\tilde{\theta}_x$ is attenuated (Fig. 4) is approximately 15% (although for a different reason); consequently, the ratios of the mean-square values are more reliable than their absolute values. The root-mean-square values of the three temperature derivatives, as well as some other relevant flow parameters are listed in Table I.

Changes are also noted in the probability density of θ_y (Fig. 6) for different values of Δy, with the more marked differences occurring essentially near the peak and the tails (shown expanded in the insets). A probability density of θ_y obtained from the four-wire probe (with Δy of $5.25\eta_\theta$, equal to the maximum value for which two-wire probe data are shown here), also plotted in Fig. 6, shows a somewhat attenuated peak and correspondingly longer tails than the probability density of θ_y from the two-wire probe for the same Δy.

One interesting feature that emerges from Fig. 5 is that the moments obtained from the four-wire probe are closer to the limiting values (corresponding to $\Delta y = 0$) than the two-wire data with the same separation distance. The explanation for this fact is to be found in Fig. 6, where the tails of the probability density for the four-wire data ($\Delta y \simeq 5.25\eta_\theta$) are seen to be closer to those of two-wire data with $\Delta y \simeq 3\eta_\theta$. It appears, therefore, that we have a fortuitous but beneficial cancellation of the effects of interference and finite separation.

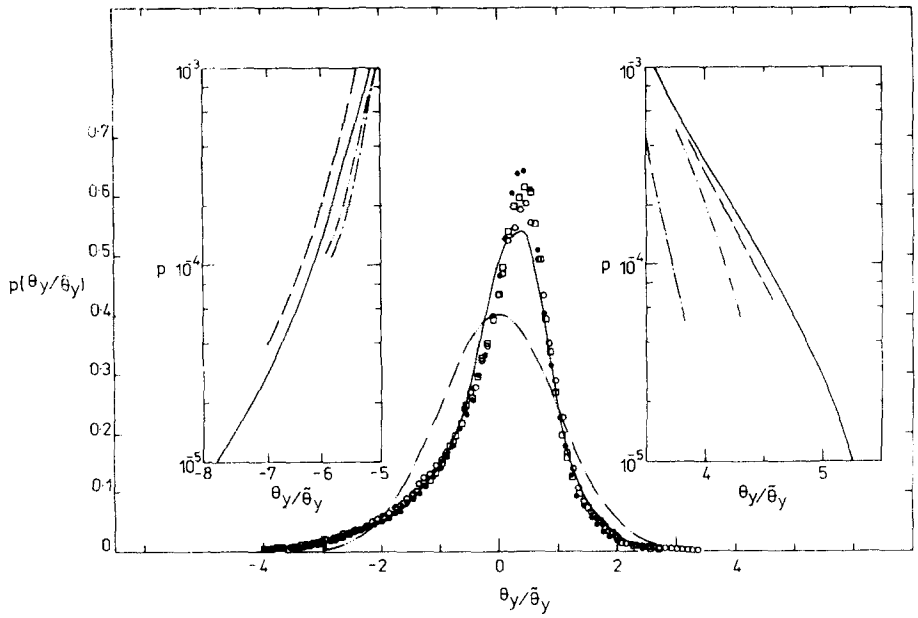

FIG. 6. Normalized probability density of θ_y from two- and four-wire probes. o, two-wire probe, $\Delta y = 5.25\eta_\theta$; □, $4.1\eta_\theta$; ●, $3\eta_\theta$; —, four-wire probe ($\Delta y = 5.25\eta_\theta$); · · · —— · · · ——, Gaussian. Details of tails are shown in insets (expanded scale). Four-wire probe: —, $\Delta y = 5.25\eta_\theta$. Two-wire probe: — —, $\Delta y = 5.25\eta_\theta$; — · · —, $4.1\eta_\theta$; — · —, $3\eta_\theta$.

Also examined in Fig. 7 are the spectral densities of θ_y with varying Δy. Clearly, there is an increased attenuation in the high frequency range as Δy increases. This attenuation is typically about 30% at a frequency corresponding to η_θ. Differences of the same order also exist for spectral density of θ_y^2 (not shown here).

Thus, there are some identifiable effects of possible probe interference on the four-wire probe data. Although they are of some significance, these discrepancies will later be shown to have no bearing on the conclusions of this work.

C. Effect of finite length of wire

Assuming isotropy and the Corrsin–Pao form for the spectral density, Wyngaard[12] estimated the wire response as a function of wire length. His calculations, with the value of 2 for the Kolmogoroff constant n as recommended by Antonia,[13] suggest that the wires used here have their −3 dB point at roughly twice the Kolmogoroff frequency. Wyngaard's estimates for the root-mean-square values of the dissipation show that they may have been underestimated by at most 15%. However, as some of the arguments used for these estimates are questionable[14] in this context, these corrections have not been incorporated here. They can, if necessary, be made using the appropriate l_w/η values quoted in Table I.

IV. STATISTICS OF DISSIPATION FLUCTUATIONS

Before we examine the statistical properties of temperature dissipation, we first note that there are marked differences between the three components of dissipation. In particular (see Fig. 8), θ_y and θ_z have less high frequency content than θ_x, and are strongly positively correlated. On the other hand, θ_x is strongly negatively correlated with θ_y or θ_z.

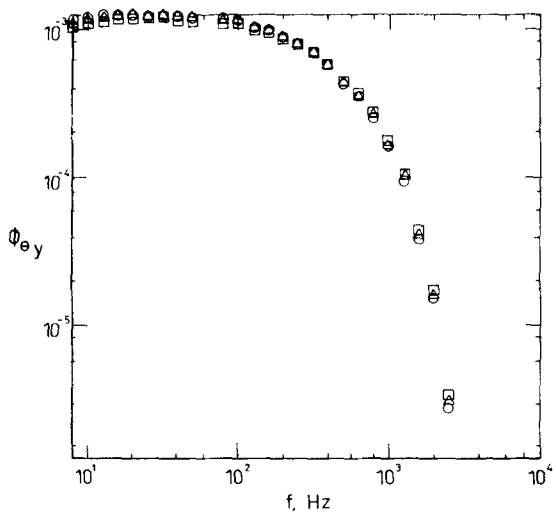

FIG. 7. Spectral density of θ_y from two wire probe for different separation distances. o, $\Delta y = 5.25\eta_\theta$; △, $4.1\eta_\theta$; □, $3\eta_\theta$.

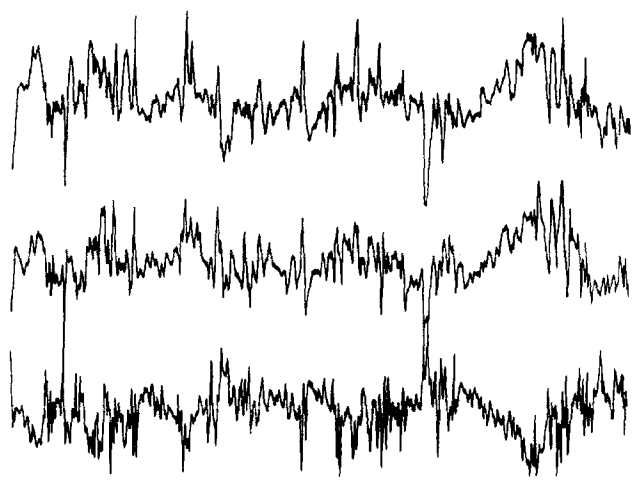

FIG. 8. Oscilloscope traces of θ_x, θ_y and θ_z, in order from below.

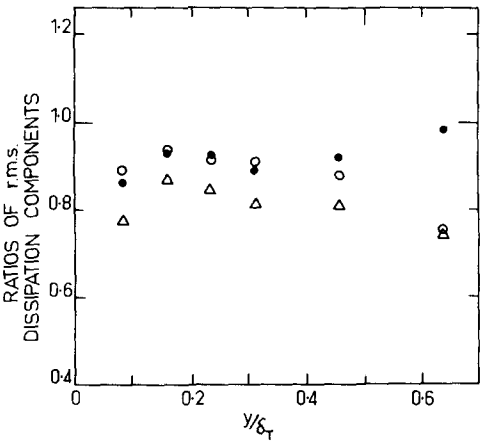

FIG. 9. Ratio of root-mean-square components of dissipation. ○, $\overline{(\theta_x^2)}^{1/2}/\overline{(\theta_y^2)}^{1/2}$; △, $\overline{(\theta_x^2)}^{1/2}/\overline{(\theta_z^2)}^{1/2}$; ●, $\overline{(\theta_y^2)}^{1/2}/\overline{(\theta_z^2)}^{1/2}$.

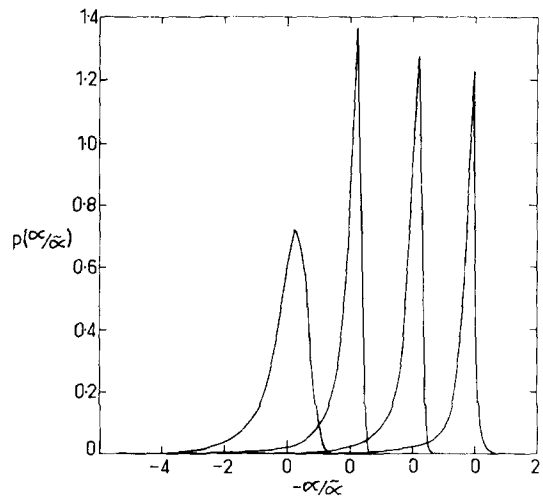

FIG. 10. Normalized probability density of χ and its components. From left to right, $\alpha = \chi - \bar{\chi}$, $\theta_y^2 - \overline{\theta_y^2}$, $\theta_z^2 - \overline{\theta_z^2}$ and $\theta_x^2 - \overline{\theta_x^2}$.

A. Mean square values

Figure 9 shows the ratio of the root-mean-square values of dissipation components. All measurements for $y \lesssim 0.6\delta_t$ show that $\overline{\theta_x^2}$ is consistently less than $\overline{\theta_y^2}$ which, in turn, is consistently less than $\overline{\theta_z^2}$.

B. Probability density

Figure 10 shows normalized probability densities of the individual as well as the sum $\chi (= \theta_x^2 + \theta_y^2 + \theta_z^2)$ of the three components of dissipation, at a typical point ($y/\delta \simeq 0.12$) in the inner layer. The most striking feature is that the sharp peak of the probability density functions of the three components is almost absent in the probability density of χ. This feature is also reflected by the skewness and flatness factors listed in Table II. The table further contains a partial summary of results at other stations, including those on the three temperature derivatives. The increase in the magnitude of the skewness and flatness factors of the individual components of dissipation with increasing y/δ is, perhaps surprisingly, not apparent in the sum. It is also interesting to note, particularly in the context of local isotropy of small scale structure, that the skewness values of θ_x and θ_y are non-zero and of order unity, while that of θ_z is nearly zero.

C. Spectral density

The lower high frequency content of θ_y^2 and θ_z^2 compared with that of θ_x^2 is clearly illustrated in the spectra shown in Fig. 11. Since the two components θ_y^2 and θ_z^2 have nearly the same spectra, it is reasonable to expect the spectral density of the sum of χ to follow more closely that of θ_y^2 and θ_z^2 than of θ_x^2. It may be argued that the spectral differences between θ_x^2 and θ_y^2 or θ_z^2 are a consequence of the "differencing" technique employed in obtaining the two latter quantities. The technique requires a finite separation to exist between the two wires, and we have seen that the high frequency content of the difference increases with decreasing separation distance (see Fig. 7). However, no better technique seems to be available for measuring θ_y and θ_z. To obtain a rough appreciation of the possible spectral attenuation due to differencing, the spectral density at a typical high frequency is obtained by simple minded linear extrapolation to $\Delta y = 0$ and indicated in Fig. 11 by a vertical bar for the θ_y^2 spectrum. Even after making such a correction, it is clear that θ_x^2 is significantly richer in high frequency than θ_y^2. This result is, in fact, consistent[15] with the concept of local isotropy.

D. Kolmogoroff's third hypothesis

Kolmogoroff[1] postulated that, at "large" Reynolds numbers, the logarithm of ϵ_r, the turbulent energy dissipation averaged over a volume of linear dimension r (such that $\eta \ll r \ll L$), has a variance $\sigma^2_{\ln \epsilon_r}$ given by

$$\sigma^2_{\ln \epsilon_r}(\mathbf{x}, t) = A(\mathbf{x}, t) + \mu \ln(L/r) ,$$

where μ is a universal constant and A depends on the large scale structure of the turbulence. The problems associated with the experimental verification of this hy-

TABLE II. Skewness and flatness factors of the three temperature derivatives, as well as of the individual components of temperature dissipation and of their sum.

	Skewness							Flatness factor						
y/δ	θ_x	θ_y	θ_z	θ_x^2	θ_y^2	θ_z^2	χ	θ_x	θ_y	θ_z	θ_x^2	θ_y^2	θ_z^2	χ
0.06	0.96	−0.96	0.07	7.48	5.94	6.05	3.03	9.25	5.60	4.77	97.87	57.70	63.55	20.10
0.12	1.00	−1.25	−0.02	8.05	5.99	6.95	3.34	9.48	6.56	7.00	103.38	51.75	82.19	21.96
0.18	0.90	−1.03	0.03	8.53	7.02	7.80	3.22	10.26	6.77	7.60	120.01	76.94	100.10	21.34
0.24	0.94	−1.09	−0.11	9.17	8.02	8.80	2.95	10.90	7.15	7.03	146.15	116.98	127.50	19.96

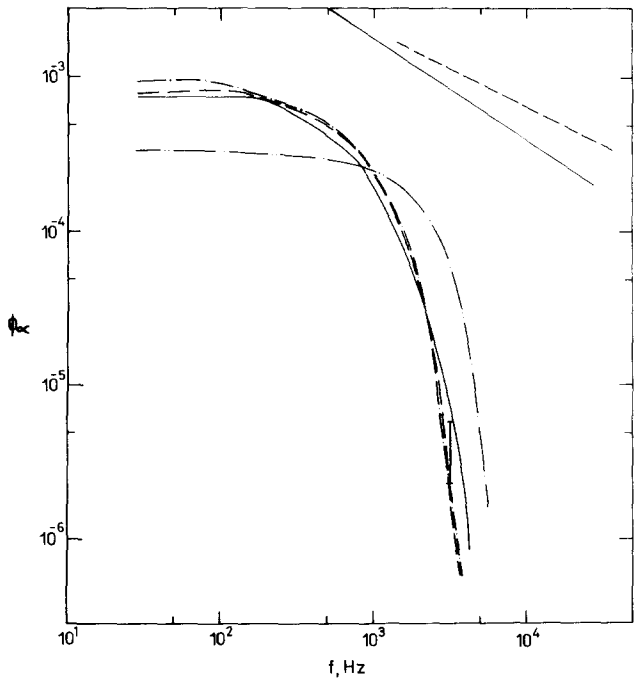

FIG. 11. Normalized frequency spectra of χ and its components. ——, χ; ——··——, θ_x^2; — —, θ_y^2; ——·——, θ_z^2. Straight lines to slopes of -0.65 (——) and -0.54 (— —).

pothesis when only one component of ϵ_r is used, and the appropriateness of testing it for χ_r, have been mentioned in Sec. I. In the case of χ_r, the variance of $\ln\chi_r$ is assumed to be given by an expression similar to that for $\sigma^2_{\ln\epsilon_r}$:

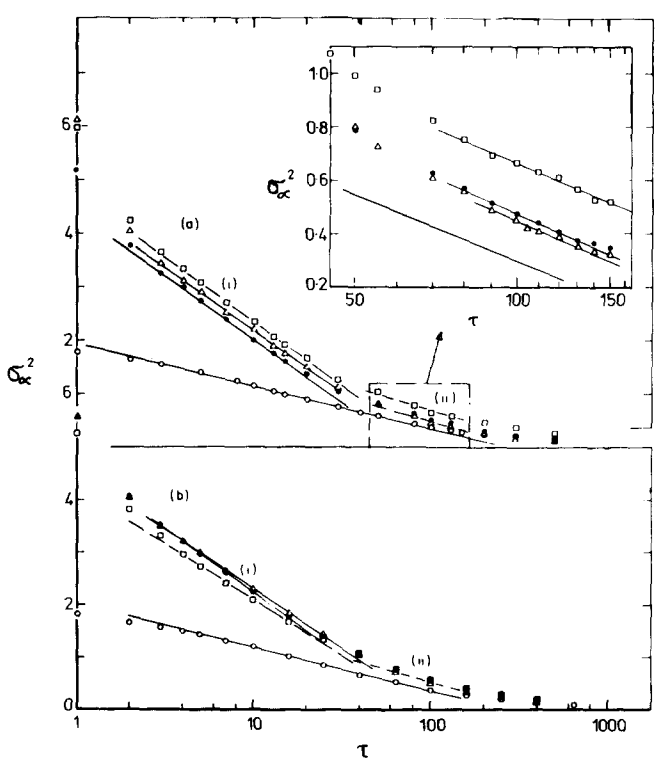

FIG. 12. Variation of σ_α^2 with τ. (a) $y/\delta = 0.06$. (b) $y/\delta = 0.12$. Region (ii) is shown in inset (expanded scale) for (a) ○, $\alpha = \Sigma$; △, X; ●, Y; □, Z.

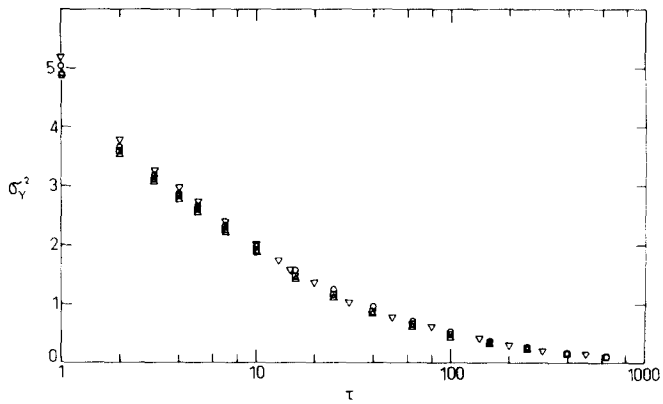

FIG. 13. Comparison of the variation of σ_Y^2 with τ, from two-wire (different Δy) and four-wire probes. ○, $\Delta y = 3\eta_\theta$; □, $4.1\eta_\theta$; △, $5.25\eta_\theta$. ▽, four-wire probe, $\Delta y = 5.25\eta_\theta$.

$$\sigma^2_{\ln\chi_\tau}(\mathbf{x}, t) = A_\theta(\mathbf{x}, t) + \mu_\theta \ln(L/r) , \tag{4}$$

where A_θ and μ_θ need not be identical to A and μ, respectively.

Consider the quantity

$$X(\tau) = \ln \frac{1}{\tau}\sum_{j=1}^{\tau} (\theta_x^2)_j - \overline{\ln \frac{1}{\tau}\sum_{j=1}^{\tau} (\theta_x^2)_j} ,$$

two other similar quantities Y and Z (with x replaced by y and z, respectively) and the quantity

$$\Sigma(\tau) = \ln \frac{1}{\tau}\sum_{j=1}^{\tau} \chi_j - \overline{\ln \frac{1}{\tau}\sum_{j=1}^{\tau} \chi_j}$$

for the sum χ, where τ is the number of sampling intervals over which averaging is performed, and is a variable. Averaging is done over mutually exclusive intervals; i.e., if $\tau = N$, the averages are taken from 1 to N, from $N+1$ to $2N$, etc. Although more sophisticated methods of averaging can be used, this simple method seems adequate here.

Figure 12 shows, for $y = 0.12\delta$, plots of the variances σ_X^2, σ_Y^2, σ_Z^2, and σ_Σ^2 as a function of τ. One noteworthy feature of this plot is that variances of the components are roughly equal and their magnitude is significantly greater than that of their sum. (If all components are identical, $\sigma_X^2 = \sigma_Y^2 = \sigma_Z^2 = \sigma_\Sigma^2$.) Further as τ increases, they decrease at a more rapid rate than σ_Σ^2. Secondly, unlike σ_Σ^2 which obeys (4) over an extensive range of τ, the individual variances exhibit some ambiguous features. For example, at least two straight-line regions exist, and the extent of both of these is one order of magnitude smaller than that for the sum.

Before we consider these results further, it is necessary to establish that they are unaffected by possible shortcomings of the data (Sec. III). Figure 13 shows that the variation of Δy does not affect σ_Y^2. The close agreement between the four-wire and two-wire data clearly proves that the differences observed in Fig. 6 are inconsequential with respect to the present discussion. Further, we have found that varying the root-mean-square values of one or two of the components (by multiplying the component signals by non-unity fac-

TABLE III. Summary of the range of r for which Eq. (4) is valid for the component and total dissipation, and the respective values of μ_θ.

y/δ	r/η							μ_θ						
	X		Y		Z		Σ	X		Y		Z		Σ
	(i)	(ii)	(i)	(ii)	(i)	(ii)		(i)	(ii)	(i)	(ii)	(i)	(ii)	
0.06	5–50	140–280	5–35	150–260	5–50	160–300	5–160	1.03	0.38	1.03	0.38	1.03	0.38	0.35
0.12	5–50	150–280	5–35	150–250	7–35	150–250	7–180	0.99	0.44	1.05	0.40	0.92	0.42	0.36
0.18	8–60	150–280	4–20	150–260	6–20	140–270	8–200	0.97	0.46	1.06	0.46	1.06	0.46	0.36
0.24	8–80	150–250	6–40	150–250	6–40	150–250	6–300	1.00	0.41	0.95	0.37	0.93	0.42	0.35

tors before summing) does not affect the distribution of σ_Σ^2 significantly.

To determine the possible effect of the variation in the spectral content of the components on the variance σ_Σ^2 we first considered three bandpassed signals from three different commercial random noise generators. The output from one of them (say number 1) was played through a bandpass filter set for 0–400 Hz while the other two (numbers 2 and 3) were bandpass filtered for 0–160 Hz. The variances (computed for $\tau = 1$) of the logarithm of the squares of these individual signals as well as of the sum of the squares, taken two at a time are as follows:

$$\sigma_1^2 = 1.71, \quad \sigma_2^2 = 1.69, \quad \sigma_3^2 = 1.63,$$

$$\sigma_{1+2}^2 = 0.71, \quad \sigma_{2+3}^2 = 0.68, \quad \sigma_{3+1}^2 = 0.70.$$

For turbulent signals X, Y, Z (taken at $y/\delta = 0.12$), the analogous results are

$$\sigma_X^2 = 5.56, \quad \sigma_Y^2 = 5.55, \quad \sigma_Z^2 = 5.25,$$

$$\sigma_{X+Y}^2 = 2.65, \quad \sigma_{Y+Z}^2 = 2.34, \quad \sigma_{Z+X}^2 = 2.73.$$

Although the variance of the logarithm of the sum of the components with similar spectral content (2 and 3 for Gaussian noise and Y and Z for turbulence) is somewhat lower than the other two, the differences seem to be marginal.

Table III summarizes the results for the range of validity of Eq. (4) and values of μ_θ in the inner layer. For the sum, the slope is unique and $\mu_\theta \simeq 0.35$ for all stations. For the components, however, the value of μ_θ depends on the part of the σ^2 vs $\ln r$ curve used for fitting a straight line. For example, in region (i), which covers the range $5\eta < r < 50\eta$, the curves have a slope of approximately -1. In a second possible region (ii) in the range $150\eta < r < 300\eta$, it varies between -0.38 and -0.46. Thus, unless we are guided by an independent criterion as to the relevant range of r to be used (such as the inertial subrange on the spectra, for instance), it is difficult to determine μ_θ from the slopes of the individual variances. Unfortunately, however, at the laboratory Reynolds numbers, determination of the inertial subrange for the spectra is generally equally ambiguous, and is masked by several features such as the digital "noise" or scatter in analog measurements. We can therefore resort only to indirect arguments for deciding the appropriate range of r, if it indeed exists, for the components.

Firstly, we note that region (i) is too close to the viscous region to be of significance for the determination of μ_θ. Secondly, the arguments of Yaglom,[4] which relate μ (or μ_θ) to the slope of the inertial subrange of the dissipation spectra, do not distinguish between the components and the sum. Purely from dimensional considerations, the slopes of the spectra of the components and their sum must be the same in a well-defined inertial subrange where it exists. Thirdly, while $\sigma_\Sigma^2 < \sigma_X^2 \simeq \sigma_Y^2 \simeq \sigma_Z^2$ we note that for sufficiently large r/η, σ_X^2, σ_Y^2, and σ_Z^2 all approach σ_Σ^2 from above (Fig. 12). This suggests that in the limit of infinite Reynolds numbers, where the relevant region of r is substantial, the values of μ (or μ_θ) for the components approach (also from above) that for the sum. As the Reynolds number is reduced, however, it is conceivable that this region of nearly identical slopes shrinks, and that any straight line region that exists for the components will only yield an upper bound for μ. There is, however, no basic reason to expect the constant μ (or μ_θ) to be vastly different for the components and the sum. The region (i) which gives apparently contradictory results must therefore be considered to be of no significance in this context.

The range of validity of Eq. (4) extends for $5\eta < r < 150\eta$ typically (a factor of 30 in r) for the sum, as against a narrower range of $150\eta < r < 300\eta$ (a factor of 2 in r) for the components. This and the comparatively unique determination of μ_θ for the sum are some of the advantages of working with χ instead of its components.

Slopes of -0.65 (appropriate to $\mu_\theta = 0.35$) and -0.54 (appropriate to $\mu_\theta = 0.46$) are drawn in Fig. 11. There exists a small range of frequencies (corresponding to $6\eta - 15\eta$) in the spectrum of the sum of which the slope is consistent with $\mu_\theta = 0.35$. The reason for the lower end (in terms of frequency) of this "inertial subrange" being much smaller than that evidenced in Fig. 12 is perhaps the high frequency attenuation of θ_y^2 and θ_z^2 due to the differencing; it is also possible that the requirements of high Reynolds number flow are more stringent for Yaglom's extension than for Kolmogoroff's third hypothesis (4). There is, in fact, no perceptible region with the "correct" slope for the individual spectra! In fact, a closer look at the spectra of the components suggests regions (in the lower frequency end) where the slope is some other constant, giving a spuriously high value for μ_θ. This emphasizes the danger of determining μ (or μ_θ) from the individual spectra obtained at low Reynolds numbers.

TABLE IV. Different estimates obtained for μ or μ_θ.

Investigators	Method	Flow	μ or μ_θ
Gurvich and Zubkovskii[19]	Slope of $(\partial w/\partial x)^2$ spectrum	Atmospheric data, height 4 m	0.38
Pond *et al.*[20]	Slope of $(\partial u/\partial x)^2$ spectrum		0.38
Pond and Stewart[21]	a. Slope of $(\partial u/\partial x)^2$ spectrum b. Damped by low pass filter	Ocean data, height 1.5 m	0.38 ± 0.02 0.62 ± 0.02
Gurvich and Yaglom[5]	Slope of variance[a] of $(\partial\theta/\partial x)_r^2$ against r	Atmospheric data, surface layer	0.4
Sheih *et al.*[18]	Slope of $(\partial u/\partial x)^2$ spectrum	Atmospheric data $R_\lambda \simeq 2280-5330$	0.70
Stewart *et al.*[22]	Slope of $(\partial u/\partial x)^2$ spectrum	Ocean data, height 2 m	0.35
Gibson *et al.*[23]	a. Slope of $(\partial u/\partial x)^2$ spectrum b. From Kolmogoroff's third hypothesis $r = \eta$	Ocean data, height 2–12 m Ocean data, height 2–12 m	0.51 ± 0.02 0.44 ± 0.25
Wyngaard and Tennekes[16]	Slope of the $(\partial u/\partial x)^2$ spectrum	Curved mixing layer, $R_\lambda \simeq 200$	0.85
Gibson and Masiello[3]	From slope of variance of $(\partial u/\partial x)_r^2$ against r. From $3\sigma^2/\ln n$.[b]	Ocean data, height 30 m	0.47 ± 0.03 0.49 ± 0.20
Friehe *et al.*[24]	Slope of $(\partial u/\partial x)^2$ spectrum	Round jet, $R_\lambda \simeq 540$	0.5
Masiello[6]	From the slope of $(\partial u/\partial x)_r^2$ and $(\partial\theta/\partial x)_r^2$ against r.	Atmospheric data from u and θ heated jet for θ	0.47–0.58
Antonia and Van Atta[17]	Slope of the variance of $(\partial u/\partial x)_r^2$ and $(\partial\theta/\partial x)_r^2$ against r.	Heated jet, $R_\lambda \simeq 200$	0.72
Present	Slope of σ_{D^2} against r. Slope of σ_{X^2}, σ_{Y^2}, σ_{Z^2} against r.	Heated boundary layer, $R_\lambda \simeq 150$	0.35 0.38–0.46

[a]Suffix r indicates averaging over a volume of linear dimension r.
[b]σ^2 is the variance of $\ln[(\partial u/\partial t)_\alpha^2/(\partial u/\partial t)_\beta^2]$, and $n = (\beta/\alpha)^3$.

To check whether the present estimates of μ_θ are consistent with those for μ and μ_θ obtained by several different methods in the literature,[5,6,16–24] they are compared in Table IV, which is essentially an updated version of that given by Gibson and Masiello.[3] Although values of the "universal" constant μ (or μ_θ) covers a broad band, a less pessimistic picture emerges if the table is viewed in the light of our previous discussion. Wyngaard and Tennekes[16] obtained 0.85 from the slope of the spectrum of $(\partial u/\partial t)^2$ at $R_\lambda \simeq 200$ ($R_\lambda = \tilde{u}\lambda/\nu$, where λ is the Taylor microscale). For reasons already explained, the procedure is unreliable at low Reynolds numbers. Antonia and Van Atta's[17] data permit an equally well defined slope of 0.35 (for both μ and μ_θ) instead of 0.70, over a different range of r/L; extending the previous arguments to energy dissipation suggests that this method is of doubtful validity when one component of dissipation is used to determine μ, at least for low Reynolds number, without an independent indicator of inertial subrange. The $(\partial u/\partial t)^2$ spectra of Sheih *et al.*[18] obtained at high Reynolds numbers in the atmosphere exhibit too much scatter to permit a unique determination of the slope. In fact, they admit many slopes including -0.6 ($\mu = 0.4$). All other investigators obtain values between 0.29 and 0.59 for μ and μ_θ. It therefore appears that the best estimate available for μ_θ (and indeed of μ) lies between 0.35 and 0.50, and is perhaps closer to the lower value. Thus, although no basic reason can at present be given for μ and μ_θ to be the same, experimental data seem to suggest that they are comparable.

E. Log-normality of dissipation

An independent assumption is the log-normality of dissipation fluctuations. Gurvich and Yaglom[5] have used plausible arguments to show that any positive definite quantity associated with the fine scale structure of turbulence is also log-normal. Figure 14(a) shows the probability of X, Y, Z, and Σ. The probability densities of the dissipation components depart strongly from log-normality, when unaveraged (i.e., $r = 1$). This is particularly evident in the tails when the measured probability density is higher than the log-normal value. At -3σ, for example, the measured probability is one order of magnitude higher. There appears to be no well-defined region where the data follow the log-normal trend. The sum, on the other hand, displays a fairly large range of σ [approximately -2σ to 2σ, or $0.03 < P(x) < 0.97$, where $P(x)$ is the cumulative probability of x]. There is good evidence, therefore, that log-normality is a better approximation for the sum than for the components.

It is possible, however, to compute a standard deviation, σ_b say, corresponding to lines of best fit on these plots. For the components, the lines of best fit extended over the range $0.40 < P < 0.98$, and excluded small ($\lesssim -0.3\sigma_b$) and large ($\gtrsim 3\sigma_b$, $P \gtrsim 0.98$) values of dissipation components. The ratio σ_b/σ is found to be equal to 0.825, 0.670, and 0.963 in the case of X, Y,

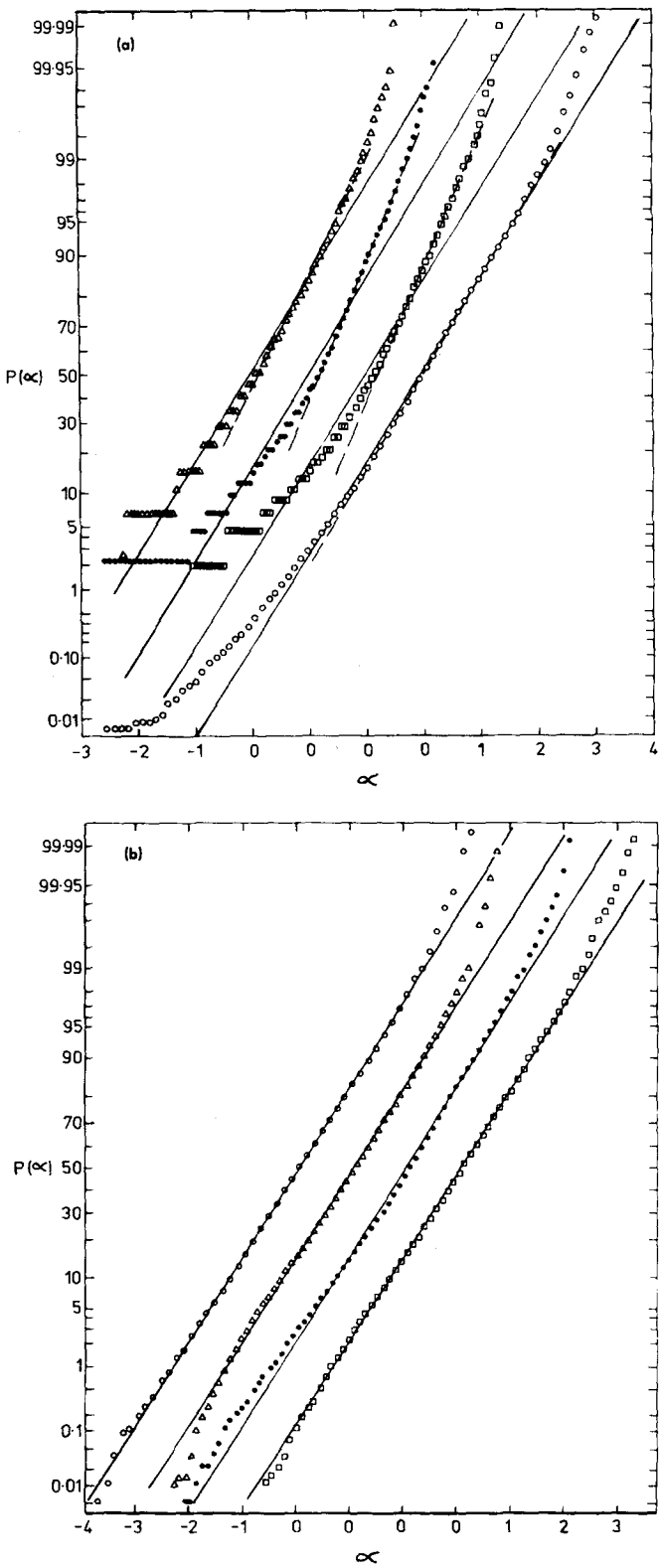

FIG. 14. Cumulative probability plots of the logarithm of dissipation and its components. ○, Σ; △, X; ●, Y; □, Z. Solid lines correspond to σ of unity. (a) $\tau = 1$; —— ——, best straight-line fit. (b) $\tau = 10$.

and Z, respectively.

Deviations from log-normality noted for $\tau = 1$ (no averaging) tend to diminish when local averaging is performed, but do not disappear altogether. These departures must be considered genuine, particularly in view of the result due to Orszag [25] that an exactly log-normal distribution for energy dissipation implies an indeterminacy of the moment problem. Data for $\tau = 10$ [Fig. 14(b)] show that there is a substantial log-normal region for the components ($-2.5\sigma_X < X < 1.5\sigma_X$, $-1.5\sigma_Y < Y < 1.5\sigma_Y$, $-3\sigma_Z < Z < 2\sigma_Z$) as well as the sum; for the latter, even the lowest probability that is recorded ($P \simeq 5\times10^{-5}$) is very close (although not exactly equal) to the log-normal value. We note that $P(Y)$ shows the worst departures for log-normality while $P(Z)$ is generally fairly close to $P(\Sigma)$. The situation is essentially unchanged (data are not shown here) for higher values of τ.

Figures 15(a) and 15(b) show the skewness and flatness factors, respectively, of X, Y, Z, and Σ, as a function of τ. For $\tau \gtrsim 5$, skewness and flatness factors, are close but not quite equal to 0 and 3, respectively. This figure reinforces our earlier conclusions that departures from log-normality do exist at all r, but diminish over a range of values of r, and that these departures are smaller for the sum than for the components, and that the probability of θ_z^2 is closer to that of the sum than the other two components.

An indication of the departures of θ_x^2, θ_y^2, θ_z^2 and χ from log-normality can be obtained as follows. If these quantities were exactly log-normal, their kurtosis (= flatness factor − 3) must be related to the variance σ_α^2 through the relation[26]

$$K_\alpha = \xi_\alpha^8 + 6\xi_\alpha^6 + 15\xi_\alpha^4 + 16\xi_\alpha^2 , \tag{5}$$

where α refers to X, Y, Z, or Σ, and $\xi_\alpha = \exp(\sigma_\alpha^2) - 1$. Values of K_α computed from Eq. (5) using σ_α^2 obtained earlier (see Fig. 12), are plotted in Fig. 16, over a range of τ, for $y = 0.12\delta$. This figure shows that at $\tau = 1$, the measured kurtosis (listed in Table II) of the components and the sum are several orders of magnitude lower than the value of K implied by Eq. (5). For the sum, however, the implied K is much smaller than for the components, but still two orders of magnitude

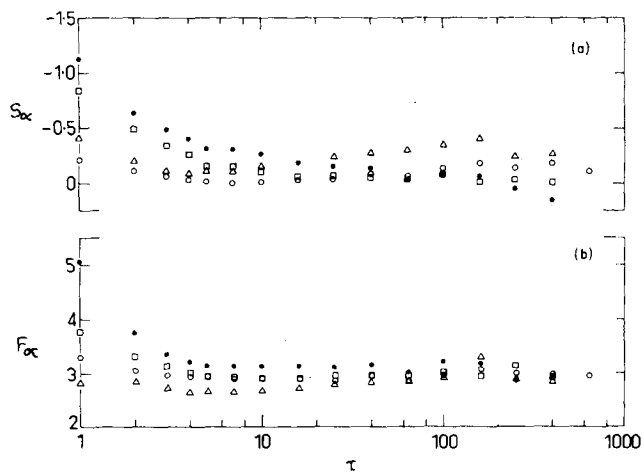

FIG. 15. Skewness and flatness factors of logarithm of dissipation and its components as a function of τ. ○, Σ; △, X; ●, Y; □, Z. (a) skewness. (b) flatness factor.

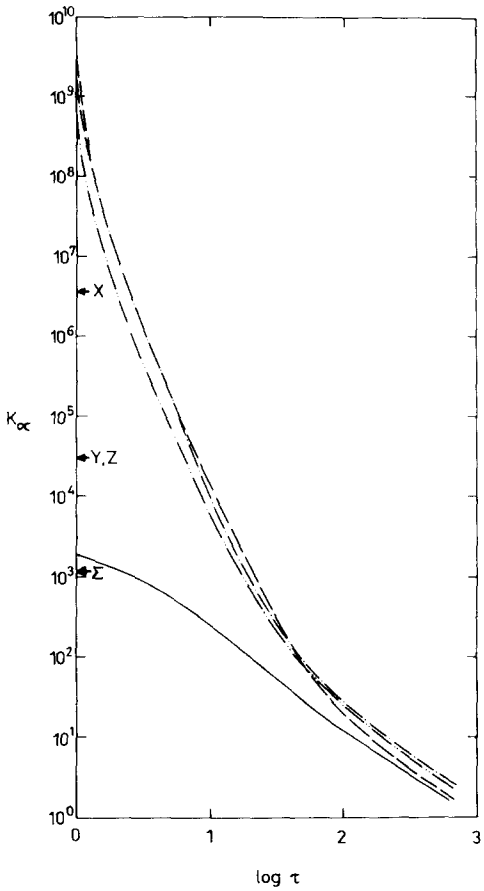

FIG. 16. Variation with τ of kurtosis K_α as implied by log-normality of α. Measured values of σ_α are used. ——, $\alpha = \Sigma$; — — —, X; ——·——, Y; ——··——, Z. Arrows refer to values K_α (with σ_b instead of σ) at $\tau = 1$.

higher than the measured values. When σ_b is used instead of σ, values of K (shown in Fig. 16 only at $\tau = 1$) are, although relatively lower than those evaluated from σ, still very much higher than the measured values.

It may be argued that the previous comparison tends to exaggerate the departure from log-normality of statistics associated with the dissipation field. Gibson *et al.*[27] and Gibson and Masiello,[3] on the other hand, use as basis for comparison the kurtosis (implied from the assumed log-normality) for the derivative rather than the square of the derivative. In Table V, a comparison is made for $\tau = 1$ between the implied value of the flatness factor of θ_x, θ_y, θ_z, and the measured values. Although the agreement is better than with K_α, large departures still exist, regardless of whether σ or σ_b is used. This latter comparison, however, seems to be physically less significant.

These implied values of K_α suggest that the signals which they represent are strongly intermittent with very high amplitudes occurring over very short intervals of time and hence require a relatively large number of samples for obtaining reliable statistics. A crude estimate for this number can be made if a highly spiked random telegraph signal of very low intermittency γ is used to model these "spikes." The flatness factor of this signal is simply γ^{-1}. If the measured flatness factors of θ_x^2, θ_y^2, θ_z^2, and χ are used for guidance, it follows that about 10^4 such peaks exist for the components, and five times as many for the sum, in a typical sample size used here. If the implied values of K_α of Fig. 16 are used instead, only about 300 such peaks exist for the sum with a significantly smaller number for the components. It would appear, therefore, that an unreasonably large number of samples, of the order of 10^{10}, is required to obtain steady statistics for the components. As reliable statistics for the sum can be obtained with a reasonable number of samples, there is an added advantage in dealing with χ instead of its individual components.

V. CONCLUDING REMARKS

Before evaluating the statistics of the dissipation χ, an assessment has been made of the experimental arrangement and techniques used to obtain the instantaneous components of χ. The finite difference approximation to θ_y and θ_z is found to have some limitations, whose overall effect shows up as a decrease in root-mean-square values and an attenuation of the high frequency end of the normalized spectra. Further, the probability densities of θ_y^2 and θ_z^2 appear to be slightly distorted. It is established, however, that these limitations do not affect the conclusions of this paper, particularly those related to the statistics of χ.

In the inner region of the boundary layer, the assumption of local isotropy of small scale turbulence does not seem to be a good approximation as $\overline{\theta_x^2} < \overline{\theta_y^2} < \overline{\theta_z^2}$. In the outer layer, the mean values of the three components of χ are nearly equal. The probability density of χ is less skewed and has a lower kurtosis than that of its components. The range of r over which Kolmogoroff's third hypothesis is valid for the sum is wide in extent ($r_{max}/r_{min} \simeq 30$) and is approximately one order of magnitude larger than for the individual components. A more definite possibility for the evaluation of the universal constant μ_θ is therefore provided by the use of the sum χ rather than the individual components of χ. The use of the individual components is somewhat ambiguous in low R_λ flows and, at best, provides upper bounds to the value of μ_θ determined from the sum. The requirement of high R_λ appears to be even more stringent in the determination of μ_θ from the slope of

TABLE V. Comparison between measured and implied (by log-normality) flatness factors of θ_x, θ_y, θ_z. Quantities in parenthesis at $y/\delta = 0.12$ are those obtained by using σ_b instead of σ.

	Flatness factor					
	θ_x		θ_y		θ_z	
y/δ	Measured	Implied	Measured	Implied	Measured	Implied
0.06	9.25	448.9	5.60	388.5	4.77	179.3
0.12	9.48	259.8 (43.9)	6.56	257.3 (12.1)	7.00	190.6 (12.0)
0.18	10.26	685.4	6.77	196.4	7.60	632.7
0.24	10.90	685.4	7.15	253.9	7.03	186.6

the dissipation spectrum in the inertial subrange. The present estimates of μ_θ are about 0.35 from the sum and in the range of 0.38–0.46 from the components. These are quite consistent with the "best" estimates for μ_θ (and μ) available in the literature.

The probability density of χ is closer to the log-normal distribution than those of its components. Departures from log-normality diminish when local averaging is performed, but do not entirely disappear. Cumulative probability plots highlight these differences. The advantages of dealing with χ instead of its components cannot be over-emphasized and it is our intention to extend these measurements to the atmospheric surface layer.

ACKNOWLEDGMENTS

We wish to thank Dr. D. Britz who developed and ran the computer program used here.

The work described in this paper represents part of a program of research supported by the Australian Research Grants Committee and the Australian Institute of Nuclear Science and Engineering.

[1]A. N. Kolmogoroff, J. Fluid Mech. **13**, 82 (1962).
[2]A. M. Obukhov, J. Fluid Mech. **13**, 77 (1962).
[3]C. H. Gibson and P. J. Masiello, in *Statistical Models and Turbulence*, edited by M. Rosenblatt and C. W. Van Atta (Springer-Verlag, Berlin, 1972), p. 427.
[4]A. M. Yaglom, Dokl. Acad. Nauk. SSSR-[Sov. Phys.-Dokl. **11**, 26 (1966)].
[5]A. S. Gurvich and A. M. Yaglom, Phys. Fluids Suppl. **10**, S59 (1967).
[6]P. J. Masiello, Ph. D. thesis, University of California, San Diego (1974).
[7]R. A. Antonia, H. Q. Danh, and A. Prabhu, J. Fluid Mech. **80**, 153 (1977).
[8]J. C. Wyngaard, J. Phys. E **2**, 1105 (1968).
[9]A. Strohl and G. Comte-Bellot, J. Appl. Mech. (Trans. ASME) **40**, 661 (1973).
[10]F. H. Champagne, V. G. Harris, and S. Corrsin, J. Fluid Mech. **41**, 81 (1970).
[11]D. J. Tritton, J. Fluid Mech. **28**, 433 (1967).
[12]J. C. Wyngaard, Phys. Fluids **14**, 2052 (1971).
[13]R. A. Antonia, Phys. Fluids **18**, 1584 (1975).
[14]J. Schedvin, G. R. Stegen, and C. H. Gibson, J. Fluid Mech. **65**, 561 (1974).
[15]C. W. Van Atta, J. Fluid Mech. (to be published).
[16]J. C. Wyngaard and H. Tennekes, Phys. Fluids **13**, 1962 (1970).
[17]R. A. Antonia and C. W. Van Atta, J. Fluid Mech. **67**, 273 (1975).
[18]C. M. Sheih, H. Tennekes, and J. L. Lumley, Phys. Fluids **14**, 201 (1969).
[19]A. S. Gurvich and S. L. Zubkhovskii, Izv. Acad. Nauk. SSSR Ser. Geofiz. **12**, 1856 (1963).
[20]S. Pond, R. W. Stewart, and R. W. Burling, J. Atmos. Sci. **20**, 319 (1963).
[21]S. Pond and R. W. Stewart, Izv. Acad. Nauk. SSSR Ser. Geofiz. **1**, 914 (1965).
[22]R. W. Stewart, J. R. Wilson, and R. W. Burling, J. Fluid Mech. **41**, 141 (1970).
[23]C. H. Gibson, G. R. Stegen, and S. McConnell, Phys. Fluids **13**, 2448 (1970).
[24]C. A. Friehe, C. W. Van Atta, and C. H. Gibson, in *Turbulent Shear Flows*, AGARD Conference Proceedings No. 93 (Advisory Group for Aerospace Research and Development, North Atlantic Treaty Organization, Neuilly sur Seine, France, 1972), p. 18-1.
[25]S. Orszag, Phys. Fluids **13**, 2211 (1970).
[26]J. Aitchison and J. A. C. Brown, *The Log-normal Distribution* (Cambridge University, Cambridge, 1957), p. 8.
[27]C. H. Gibson, G. R. Stegen, and R. B. Williams, J. Fluid Mech. **41**, 153 (1970).